

# Biphasic activation of $\beta$ -arrestin 1 upon interaction with a GPCR revealed by methyl-TROSY NMR

Yutaro Shiraishi<sup>1</sup>, Yutaka Kofuku<sup>2</sup>, Takumi Ueda<sup>2</sup>, Shubhi Pandey<sup>3</sup>, Hemlata Dwivedi-Agnihotri<sup>3</sup>, Arun K. Shukla<sup>3</sup> & Ichio Shimada<sup>1</sup>✉

$\beta$ -arrestins ( $\beta$ arrestins) play multifaceted roles in the function of G protein-coupled receptors (GPCRs).  $\beta$ arrestins typically interact with phosphorylated C-terminal tail (C tail) and transmembrane core (TM core) of GPCRs. However, the effects of the C tail- and TM core-mediated interactions on the conformational activation of  $\beta$ arrestins have remained elusive. Here, we show the conformational changes for  $\beta$ arrestin 1 activation upon the C tail- and TM core-mediated interactions with a prototypical GPCR by nuclear magnetic resonance (NMR) spectroscopy. Our NMR analyses demonstrated that while the C tail-mediated interaction alone induces partial activation, in which  $\beta$ arrestin 1 exists in equilibrium between basal and activated conformations, the TM core- and the C tail-mediated interactions together completely shift the equilibrium toward the activated conformation. The conformation-selective antibody, Fab30, promotes partially activated  $\beta$ arrestin 1 into the activated-like conformation. This plasticity of  $\beta$ arrestin 1 conformation in complex with GPCRs engaged in different binding modes may explain the multifunctionality of  $\beta$ arrestins.

<sup>1</sup>Laboratory for Dynamic Structure of Biomolecules, RIKEN Center for Biosystems Dynamics Research (BDR), 1-7-22 Suehiro-cho, Tsurumi-ku, Yokohama, Kanagawa 230-0045, Japan. <sup>2</sup>Graduate School of Pharmaceutical Sciences, The University of Tokyo, Hongo 7-3-1, Bunkyo-ku, Tokyo 113-0033, Japan. <sup>3</sup>Department of Biological Sciences and Bioengineering, Indian Institute of Technology, Kanpur 208016, India. ✉email: [ichio.shimada@riken.jp](mailto:ichio.shimada@riken.jp)

After activation by agonist binding, G protein-coupled receptors (GPCRs) are typically phosphorylated at serine and/or threonine residues on their C-terminal region by GPCR kinases (GRKs), and  $\beta$ -arrestins ( $\beta$ arrests) bind to the phosphorylated GPCRs, leading to signal regulation via GPCRs.  $\beta$ arr binding to GPCRs elicits multifaceted responses such as receptor desensitization, receptor internalization, and activation of mitogen-activated protein kinases (MAPKs). The functions of  $\beta$ arrests are driven by scaffolds of various downstream effectors, such as clathrin, adaptin, kinases, and phosphatases. The ability of GPCR-bound  $\beta$ arr to engage different scaffolding partners suggests that  $\beta$ arr can adopt multiple conformations, which are modulated by GPCRs<sup>1</sup>. Recent reports suggested that the multiple functions of  $\beta$ arr, such as desensitization, internalization, and signal transduction, could be separable by mutations of  $\beta$ arrests or ligands bound to GPCRs, and different readouts of  $\beta$ arr functions resulted in distinct pharmacological outcomes<sup>2–5</sup>. Thus, the interactions between GPCRs and  $\beta$ arrests are emerging as a focal point for drug discovery, and the details of the conformational states of  $\beta$ arrests bound to GPCRs should be clarified to provide information for developing functionally selective drugs.

$\beta$ arrests are composed of N and C lobes, and each forms a  $\beta$ -strand sandwich structure. The N and C lobes are connected by a hinge region, and the finger loop is located near the interface between the N and C lobes<sup>6</sup>.  $\beta$ arrests bind to two distinct elements in GPCRs: the carboxyl terminal region phosphorylated by GRKs (also referred to as “C tail”), and the cytoplasmic face of the agonist-activated transmembrane region (also referred to as “TM core”) <sup>7</sup>. Structural analyses revealed that the finger loop and N lobe of  $\beta$ arrests bind to the TM core and C tail of GPCRs, respectively<sup>8–12</sup>. Due to the biphasic nature of the interaction, the effects of the C tail- and TM core-mediated interactions on the conformation of  $\beta$ arrests should be separately investigated to understand their specific conformational activations. Growing evidence has suggested that the C tail interaction alone can induce signal transduction at least for some pathways<sup>2,4</sup>. Furthermore, recent studies have indicated that the TM core can activate  $\beta$ arr without the C tail-mediated interaction<sup>13,14</sup>. These findings suggest that the C tail- and TM core-mediated interactions could induce the conformational changes of  $\beta$ arrests. However, the effects of these interactions on the conformational changes for  $\beta$ arr activation in solution have remained elusive, because activated arrestin is inherently dynamic<sup>15</sup> and the available structures have been visualized with stabilization methods, including pre-activated mutants<sup>8,10,12</sup>, fusion proteins with a GPCR<sup>8,12</sup>, and the conformation-selective antibody fragment, Fab30<sup>9,11,12</sup>.

Nuclear magnetic resonance (NMR) spectroscopy is a promising approach for analyzing relationships between dynamic structural information and functions of biomolecules in solution. Here, we investigated the conformational changes of  $\beta$ arr1 induced by C tail- and TM core-mediated interactions with GPCRs by methyl transverse relaxation-optimized spectroscopy (TROSY). We also assessed the effect of the synthetic antibody Fab30 on the conformation of  $\beta$ arr1. Our results suggest that both the C tail- and TM core-mediated interactions with GPCRs are required for the full conformational changes for  $\beta$ arr1 activation in solution, and that Fab30 promotes the conformational changes for  $\beta$ arr1 activation without the TM core-mediated interactions with GPCRs. This conformational plasticity of  $\beta$ arr1 in complex with a GPCR may explain its ability to engage multiple scaffolding partners and in turn mediate distinct functional outcomes.

## Results

**Phosphorylation- and agonist-dependent interactions between  $\beta$ arr and GPCRs.** To prevent intra- and intermolecular disulfide bond formation and enhance the stability of  $\beta$ arr1, we used its

cysteine-less variant, which showed similar receptor-binding activity to wild-type  $\beta$ arr1<sup>16</sup>. We also used a modified  $\beta_2$  adrenergic receptor ( $\beta_2$ AR) construct with its C-terminus replaced by that of arginine-vasopressin type2 receptor (V2R), referred to as  $\beta_2$ V<sub>2</sub>R. This receptor construct reportedly has higher affinity for  $\beta$ arr1 than wild-type  $\beta_2$ AR, and thus was used in previous structural analyses of the GPCR–arrestin complex<sup>2,17–19</sup>. The chimeric receptor with the V2R C-terminus also allowed us to use the conformation-selective antibody fragment Fab30, which was employed in previous studies to elucidate the activated conformation structures of  $\beta$ arr1<sup>9,11,20</sup>. Since arrestins reportedly interact with membrane lipids when bound to GPCRs<sup>9,10,21</sup>, purified  $\beta_2$ V<sub>2</sub>R was embedded within a lipid bilayer of reconstituted high-density lipoproteins (rHDLs)<sup>22</sup>. Considering the facts that acidic lipids reportedly play critical roles in GRK-mediated phosphorylation and arrestin recruitment, and most physiological membranes have a negative net charge, we used a lipid mixture containing acidic lipids to construct rHDLs<sup>23–25</sup>. The reconstituted  $\beta_2$ V<sub>2</sub>R in rHDLs was phosphorylated by GRK2 in a ligand-dependent manner (Supplementary Fig. 1). To prepare phosphorylated  $\beta_2$ V<sub>2</sub>R in rHDLs bound to the inverse agonist, we phosphorylated  $\beta_2$ V<sub>2</sub>R in rHDLs bound to the full agonist, formoterol, by GRK2, and then added excess amounts of the inverse agonist, carazolol, and incubated the reaction until ligand exchange was completed (Fig. 1a, see Methods for details). We confirmed that this procedure results in bound ligand exchange from formoterol to carazolol by monitoring the M82 methyl group resonance of phosphorylated  $\beta_2$ V<sub>2</sub>R, which exhibited distinctly different chemical shifts between the formoterol- and carazolol-bound states (Supplementary Fig. 2).

The interaction between  $\beta_2$ V<sub>2</sub>R in rHDLs and  $\beta$ arr1 was analyzed by surface plasmon resonance (SPR) experiments. The responses of  $\beta$ arr1 to unphosphorylated  $\beta_2$ V<sub>2</sub>R in rHDLs bound to the full agonist were essentially the same as those to empty rHDLs, suggesting that unphosphorylated  $\beta_2$ V<sub>2</sub>R in rHDLs has low affinity for  $\beta$ arr1 (Fig. 1b; middle and right). In contrast, the injection of  $\beta$ arr1 into phosphorylated  $\beta_2$ V<sub>2</sub>R in rHDLs elicited larger responses, suggesting that phosphorylated  $\beta_2$ V<sub>2</sub>R in rHDLs has higher affinity for  $\beta$ arr1 than unphosphorylated  $\beta_2$ V<sub>2</sub>R in rHDLs as expected (Fig. 1b; left and middle). The potentiation of  $\beta$ arr1 affinity upon  $\beta_2$ V<sub>2</sub>R phosphorylation in rHDLs suggests that  $\beta$ arr1 binds to the phosphorylated C tail of  $\beta_2$ V<sub>2</sub>R in rHDLs. Next, to investigate the effect of ligand efficacy on the TM core interaction, we analyzed  $\beta$ arr1 binding to phosphorylated  $\beta_2$ V<sub>2</sub>R in rHDLs bound to full and inverse agonists by SPR experiments. Injections of high concentrations of  $\beta$ arr1 (2.0, 4.0, and 8.0  $\mu$ M) resulted in serious non-specific binding to the sensor chip surface, thus hampering quantitative analyses of the specific interactions with the receptor (Supplementary Fig. 3). Therefore, the experiments were carried out with a lower concentration range (0.031, 0.063, 0.13, 0.15, 0.5, and 1.0  $\mu$ M). Steady-state analyses showed that phosphorylated  $\beta_2$ V<sub>2</sub>R in rHDLs bound to the inverse agonist had lower affinity for  $\beta$ arr1 ( $K_d > 1 \mu$ M) than that bound to the full agonist ( $K_d = 0.24 \pm 0.01 \mu$ M) (Fig. 1C and D). Since the same phosphorylation states of full agonist- and inverse agonist-bound  $\beta_2$ V<sub>2</sub>R in rHDLs were used, the observed affinity variance for  $\beta$ arr1 is strictly due to differences in the ligands bound to the TM core. Furthermore, while the resonances from M215 and M279, located on the intracellular side of the TM core, reportedly exhibited significant chemical shift changes upon  $\beta$ arr1 binding in the full agonist-bound state<sup>26</sup>, such changes were not observed upon  $\beta$ arr1 binding in the inverse agonist-bound state (Supplementary Fig. 4), suggesting that  $\beta$ arr1 binding to the TM core is modulated by the ligand efficacy. Therefore, the possibility remains that the C tail undergoes conformational changes in a ligand-dependent manner and subsequently affects

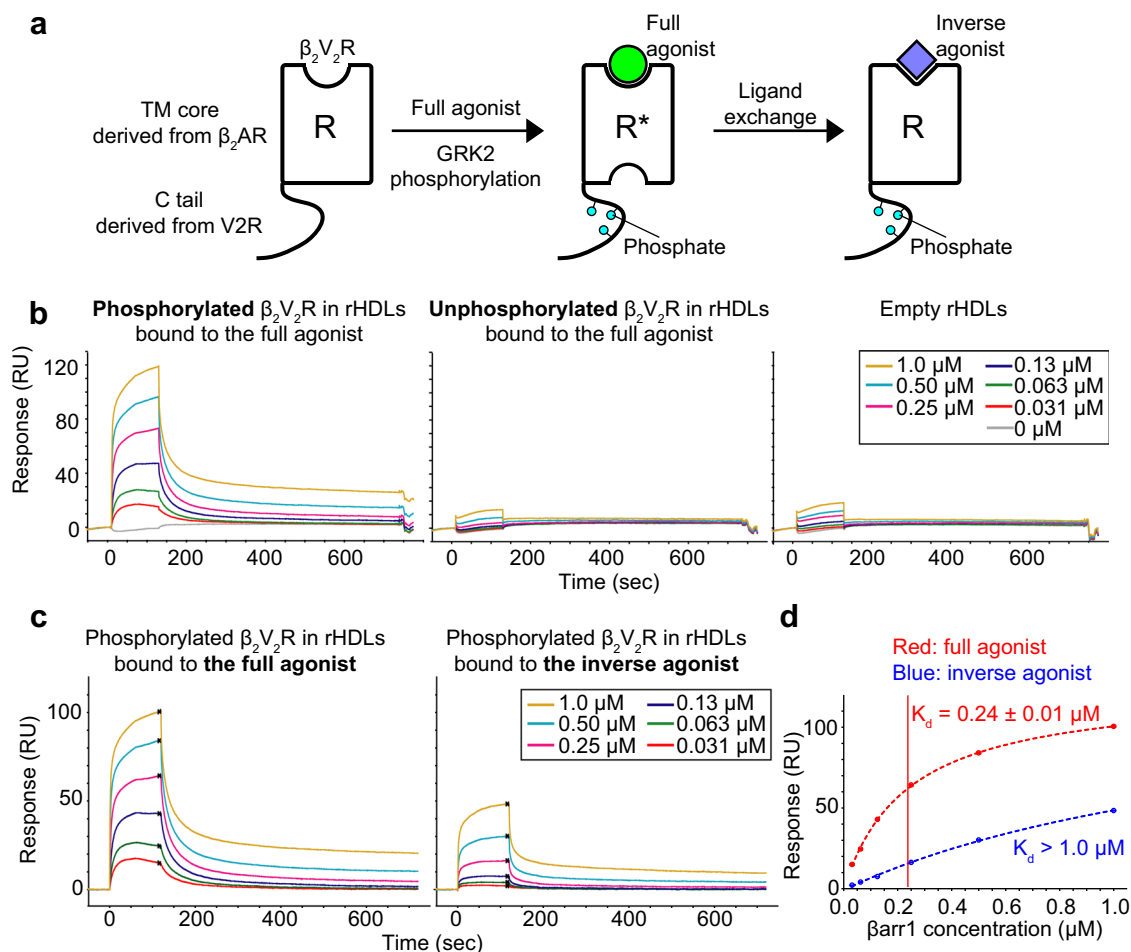


**Fig. 1** SPR analyses of the interactions between  $\beta$ arr1 and  $\beta_2V_2R$  in rHDLs. **a** Schematic representation of the various forms of  $\beta_2V_2R$ , composed of the TM core from  $\beta_2AR$  and the C tail from  $V_2R$ , used in this study. Purified  $\beta_2V_2R$ s in rHDLs bound to the full agonist are phosphorylated by GRK2. Afterwards, the full agonist was replaced with the inverse agonist. **b** Overlay plots of sensorgrams obtained for the interactions of 0, 0.031, 0.063, 0.13, 0.25, 0.50, and 1.0  $\mu$ M  $\beta$ arr1 with unphosphorylated  $\beta_2V_2R$  in rHDLs (left), phosphorylated  $\beta_2V_2R$  in rHDLs (middle), and empty rHDLs (right). **c** Overlay plots of sensorgrams obtained for the interactions of 0.031, 0.063, 0.13, 0.25, 0.50, and 1.0  $\mu$ M  $\beta$ arr1 with phosphorylated  $\beta_2V_2R$  in rHDLs bound to the full agonist (left) and those bound to the inverse agonist (right). To accurately extract the ligand effects, sensorgrams from the reference flow cell immobilized with empty rHDLs were subtracted from those of the active flow cells immobilized with phosphorylated  $\beta_2V_2R$  in rHDLs, and then the sensorgrams from buffer blank injections were subtracted from the reference-subtracted sensorgrams to yield the double-referenced sensorgrams. **d** Plots based on steady-state SPR methods between  $\beta$ arr1 and phosphorylated  $\beta_2V_2R$  in rHDLs bound to the full agonist (red) and the inverse agonist (blue). Each point is the average of 50 data points around the steady state in the sensorgram, and the error bars are their standard deviations. The  $K_d$  values were determined by fitting the steady-state response curves, assuming a 1:1 interaction mode.

the interaction with  $\beta$ arr1, it is more likely that  $\beta$ arr1 binds to the TM core of  $\beta_2V_2R$  in rHDLs in a ligand efficacy-dependent manner. Accordingly,  $\beta$ arr1 and  $\beta_2V_2R$  in rHDLs retain the biphasic interaction mode.

**Conformational change of  $\beta$ arr1 induced by both TM core and C tail interactions.** To gain insight into  $\beta_2V_2R$ -induced activation of  $\beta$ arr1, we observed NMR spectra of  $\beta$ arr1 in complex with  $\beta_2V_2R$  in rHDLs. Since the  $\beta$ arr1- $\beta_2V_2R$  complex embedded in rHDLs has an apparent molecular mass of over 200 kDa, we adopted methyl-selective labeling strategies and applied methyl-TROSY techniques<sup>27</sup>. We prepared isoleucine (Ile)  $\delta$ 1- $^{13}C$ H-labeled and otherwise perdeuterated  $\beta$ arr1<sup>28</sup>, and analyzed their  $^1H$ - $^{13}C$  heteronuclear multiple-quantum coherence (HMQC) spectra.  $\beta$ arr1 possesses fifteen Ile residues widely distributed throughout its whole structure (Fig. 2a). Resonance assignments of the fifteen Ile  $\delta$ 1 methyl groups were accomplished by comparing the  $^1H$ - $^{13}C$  HMQC spectra of fifteen individual Ile mutants with that of the parental  $\beta$ arr1 construct (Supplementary Fig. 5).

First, we analyzed the conformation of  $\beta$ arr1 without receptors. In the absence of receptors,  $\beta$ arr1 adopts the basal state, in which the inactive conformation is maintained and no signal transduction activity is detected<sup>6</sup>. In the basal state, well-resolved resonances derived from the Ile  $\delta$ 1 methyl groups of  $\beta$ arr1 were observed in the  $^1H$ - $^{13}C$  HMQC spectrum (Fig. 2b; left). The resonances from I241 and I317, located on the interface between the N- and C-lobes, were split into two resonances, suggesting that this region exchanges between at least two conformations on a slower timescale than that of the chemical shift difference (Fig. 2b; left). The  $\delta$ 1 methyl group of I377, within the C-terminal region, had an exceptionally narrower resonance than the other methyl groups, indicating the high flexibility of this region (Fig. 2b; left). This observation is in agreement with the fact that the C-terminal region including I377 is disordered in the crystal structure of  $\beta$ arr1 in the basal state (Fig. 2a)<sup>6</sup>.

In the  $^1H$ - $^{13}C$  HMQC spectrum of  $\beta$ arr1 in the complex with phosphorylated  $\beta_2V_2R$  in rHDLs bound to the full agonist, the overall intensity of the resonances was lower than that in the

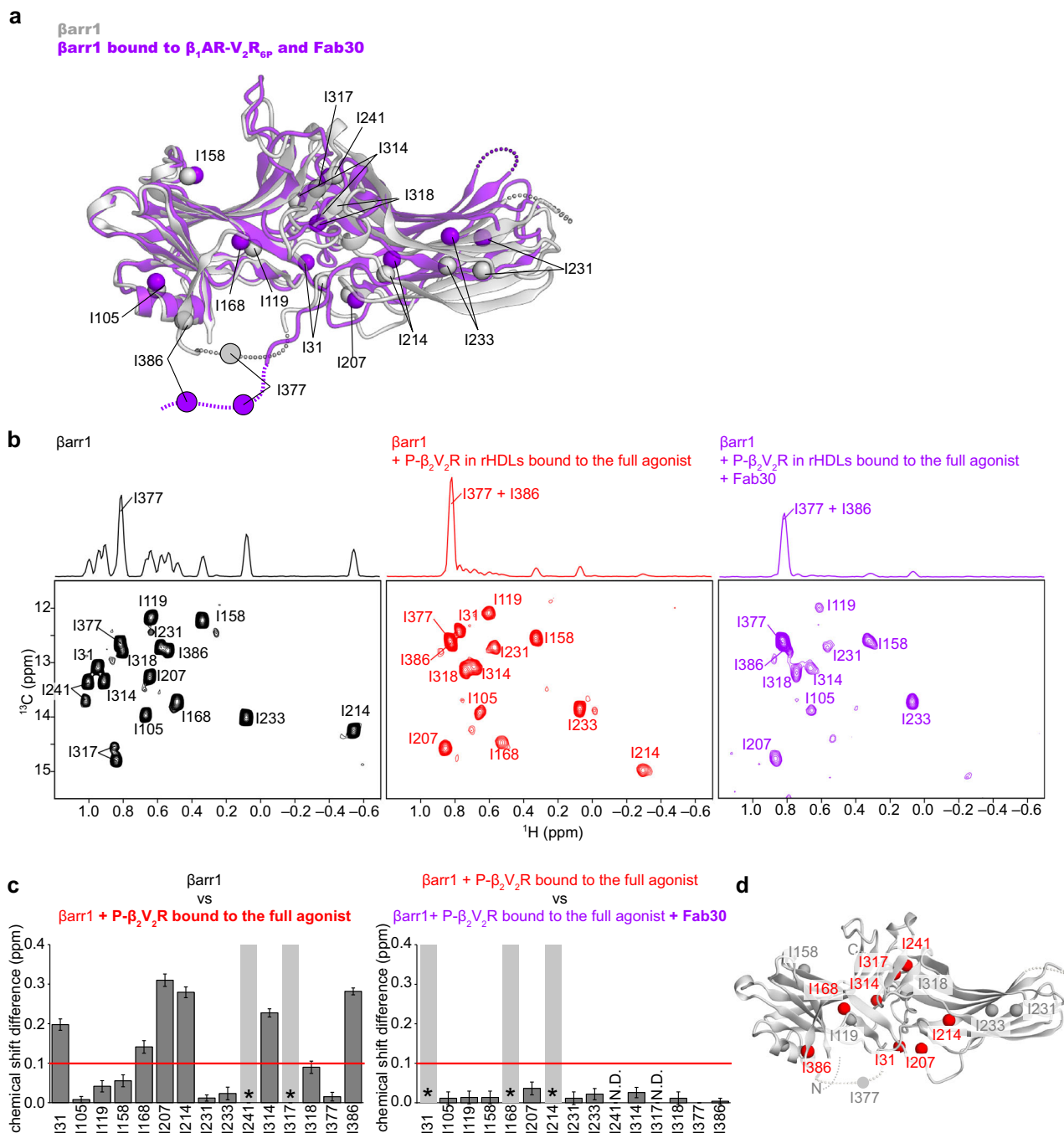


**Fig. 2** Conformational changes of  $\beta$ arr1 upon binding to phosphorylated  $\beta_2V_2R$  in rHDLs bound to the full agonist. **a** Structural differences of  $\beta$ arr1 between the basal state (gray, PDB ID: 1G4M) and in complex with  $\beta_1$ AR- $V_2R_{6P}$  and Fab30 (purple, PDB ID: 6TKO). The structural model was prepared with Cuemol (<http://www.cuemol.org/>). **b**  $^1H$ - $^{13}C$  HMQC spectra of [ $u$ - $^2H$ , Ile $\delta$ 1- $^{13}C$  $^1H_3$ ]  $\beta$ arr1 in the basal state (left, black), the complex with phosphorylated  $\beta_2V_2R$  in rHDLs bound to the full agonist (middle, red), and the complex with both phosphorylated  $\beta_2V_2R$  in rHDLs bound to the full agonist and Fab30 (right, purple). **c** Normalized chemical shift differences between the basal state and the complex with phosphorylated  $\beta_2V_2R$  in rHDLs bound to the full agonist (left), and those between the complex with phosphorylated  $\beta_2V_2R$  in rHDLs bound to the full agonist and the complex with both phosphorylated  $\beta_2V_2R$  in rHDLs bound to the full agonist and Fab30 (right). Asterisks indicate residues with resonances broadened beyond detection upon the addition of phosphorylated  $\beta_2V_2R$  in rHDLs bound to the full agonist (left) and those upon the addition of Fab30 (right). N.D. indicates residues with resonances that were not observed both before (B; middle) and after (B; right) Fab30 addition. The error bars were calculated based on the digital resolution of the spectra, as described in “Methods”. **d** Distribution of the isoleucine residues on the structure of  $\beta$ arr1 in the basal state (PDB ID: 1G4M). The residues with resonances exhibiting chemical shifts larger than 0.1 ppm upon binding to phosphorylated  $\beta_2V_2R$  in rHDLs bound to the full agonist are shown as red spheres.

spectrum of  $\beta$ arr1 in the basal state, due to an increase in the apparent molecular mass upon complex formation (Fig. 2b; middle). To determine whether this conformational change was induced by lipids alone, the interactions between  $\beta$ arr1 and empty

rHDLs, lacking phosphorylated  $\beta_2V_2R$ , were investigated. No spectral change was detected upon the addition of excess amounts of empty rHDLs to  $\beta$ arr1 (Supplementary Fig. 6). These results suggest that the conformational change of  $\beta$ arr1 is not induced by

interactions with lipids alone, but by those with phosphorylated  $\beta_2V_2R$  in rHDLs. To identify which part of  $\beta arr1$  underwent conformational changes upon complex formation, we calculated the chemical shift differences for the Ile  $\delta 1$  methyl groups resonances between the basal state and in the complex with phosphorylated  $\beta_2V_2R$  in rHDLs bound to the full agonist. Significant chemical shift differences larger than 0.1 ppm were observed for I31, I168, I207, I214, I314, and I386, which are distributed around the interface between the N- and C-lobes (Fig. 2c; left and D). In addition, the resonances from I241 and I317, located on the interface between the N- and C-lobes, were broadened beyond detection in the complex with phosphorylated  $\beta_2V_2R$  in rHDLs bound to the full agonist (Fig. 2b; middle). These spectral changes suggested that a conformational change occurred on the interface between the N- and C-lobes of  $\beta arr1$  upon binding to phosphorylated  $\beta_2V_2R$  in rHDLs bound to the full agonist (Fig. 2d). Furthermore, the  $\delta 1$  methyl groups of I377 and I386, within the C-terminal region, had exceptionally narrower resonances than other methyl groups in the complex with phosphorylated  $\beta_2V_2R$  in rHDLs bound to the full agonist, indicating that this region is highly flexible (Fig. 2b; middle and Supplementary Fig. 7). Particularly, the resonance from I386 in the complex with phosphorylated  $\beta_2V_2R$  in rHDLs bound to the full agonist was narrower than that in the basal state, indicating that the region including I386 becomes highly flexible upon this interaction (Fig. 2b; middle). This agrees well with the fact that the C-terminal region of  $\beta arr1$  is released from the N-domain of  $\beta arr1$  upon interactions with phosphorylated GPCRs (Fig. 2a)<sup>20,29</sup>.

To compare the conformation of  $\beta arr1$  in the complex with phosphorylated  $\beta_2V_2R$  in rHDLs bound to the full agonist, observed in our NMR experiments, to the activated conformations previously determined by crystallography and cryo-EM, we used the synthetic antibody fragment, Fab30<sup>9,11,20</sup>. Fab30 specifically recognizes and stabilizes the activated conformation of  $\beta arr1$ , and thus is useful to obtain the NMR spectrum corresponding to the activated conformation<sup>20</sup>. The addition of Fab30 to  $\beta arr1$ , in the complex with phosphorylated  $\beta_2V_2R$  in rHDLs bound to the full agonist, induced further intensity reductions and small chemical shift changes in some resonances, suggesting that Fab30 binds to  $\beta arr1$  in this complex (Fig. 2b; right). However, the observed chemical shift changes upon Fab30 binding were less than 0.04 ppm, and much smaller than those observed upon complex formation with phosphorylated  $\beta_2V_2R$  in rHDLs bound to the full agonist (Fig. 2c; right). These results suggest that the conformation of  $\beta arr1$ , in the complex with phosphorylated  $\beta_2V_2R$  in rHDLs bound to the full agonist and in the absence of Fab30, is similar to the activated conformation previously determined in the complex with Fab30<sup>9,11,20</sup>.

**Partial activation of  $\beta arr1$  induced by phosphorylated  $\beta_2V_2R$  bound to the inverse agonist.** To gain insight into the contributions of the TM core and C tail interactions to the conformational change for  $\beta arr1$  activation, we obtained the methyl-TROSY spectrum of  $\beta arr1$  in the complex with phosphorylated  $\beta_2V_2R$  in rHDLs bound to the inverse agonist (Fig. 3a). Under these conditions, while the phosphorylation states of the C tail remained the same, the TM core interaction was attenuated relative to the full agonist-bound state, as revealed by the SPR experiments described above (Fig. 1c; right). The result showed that the I158 resonance, in the complex with phosphorylated  $\beta_2V_2R$  in rHDLs bound to the inverse agonist, exhibited a chemical shift corresponding to that in the activated conformation (Fig. 3b; upper row). Furthermore, the resonances from I241 and

I317, in the complex with phosphorylated  $\beta_2V_2R$  in rHDLs bound to the inverse agonist, were broadened beyond detection, in a similar manner to those in the activated conformation (Fig. 3b; middle and lower rows). These observations suggested that the local environments near the phosphate-binding and TM core-binding regions adopt activated conformations (Fig. 3c). In contrast, the resonances from I119, I168, I214, I231, I314, and I318 exhibited chemical shifts corresponding to the basal conformation, while those from I31, I105, I207, I233, and I386 split into two resonances, one corresponding to the basal conformation and the other to the activated conformation (Fig. 3a). These results suggested that the attenuated core interaction induced by the inverse agonist results in partial activation. In other words, the whole  $\beta arr1$  structure, except for the phosphate- and TM core-binding regions, exists in equilibrium between the major basal and minor activated conformations.

**Effects of Fab30 on  $\beta arr1$  in the complex with phosphorylated  $\beta_2V_2R$  bound to the inverse agonist.** Our NMR analyses of  $\beta arr1$  in complex with  $\beta_2V_2R$  in rHDLs bound to full- and inverse agonists suggested that while the  $\beta arr1$  structure adopts the activated conformation in the presence of both the TM core and C tail interactions, the attenuation of the TM core interaction destabilizes the activated conformation. In contrast, the crystal structure of  $\beta arr1$  in complex with a phosphopeptide derived from V2R (V2Rpp) and Fab30, in which the TM core interactions do not exist, revealed the activated conformation<sup>20</sup>. To determine the reason for this difference, we used methyl-TROSY NMR to investigate whether the conformational change could occur, in  $\beta arr1$  in the complex with phosphorylated  $\beta_2V_2R$  in rHDLs bound to the inverse agonist, upon Fab30 addition. Interestingly, all resonances corresponding to the basal state disappeared upon the addition of Fab30 (Fig. 4a). Furthermore, some resonances, such as I105 and I233, which split into two resonances, completely shifted to those corresponding to the activated conformation (Fig. 4b). These results suggested that, although the TM core interaction is attenuated by the inverse agonist, Fab30 binding promotes  $\beta arr1$  to adopt the activated-like conformation, in which some parts are similar to those of the activated conformation. This is in agreement with the crystal structure of the  $\beta arr1$ -V2Rpp-Fab30 complex.

## Discussion

GPCR-arrestin complexes are flexible and thus several stabilization methods, such as the use of a GPCR-arrestin fusion protein<sup>8,12</sup>, a pre-activated form of arrestin<sup>8,10-12</sup>, or a conformation-selective antibody fragment, Fab30<sup>9,11,12</sup>, have been utilized to obtain the high resolution structures. Although these methods have provided excellent snapshots of the finally formed complexes, the process of complex formation and conformational activation of arrestins in solution has remained elusive. In this present study, we investigated the interaction between  $\beta arr1$  and  $\beta_2V_2R$  by SPR, and the conformational changes for  $\beta arr1$  activation without any pre-activated mutation upon binding to  $\beta_2V_2R$  embedded in a lipid bilayer, which significantly affects the complex formation<sup>9,11,21</sup>, by NMR in a near-physiological solution environment. While  $\beta arr1$  exhibited little or no affinity for unphosphorylated  $\beta_2V_2R$  in rHDLs bound to the full agonist, it exhibited higher affinity for phosphorylated  $\beta_2V_2R$  in rHDLs bound to the inverse agonist, as determined by SPR experiments (Fig. 1b; middle, and C; right). These results suggest that the affinity of  $\beta arr1$  for the phosphorylated C tail is much higher than that for the TM core bound to the full agonist. Our NMR analyses revealed that the inverse agonist-induced attenuation of the TM core interaction destabilized the

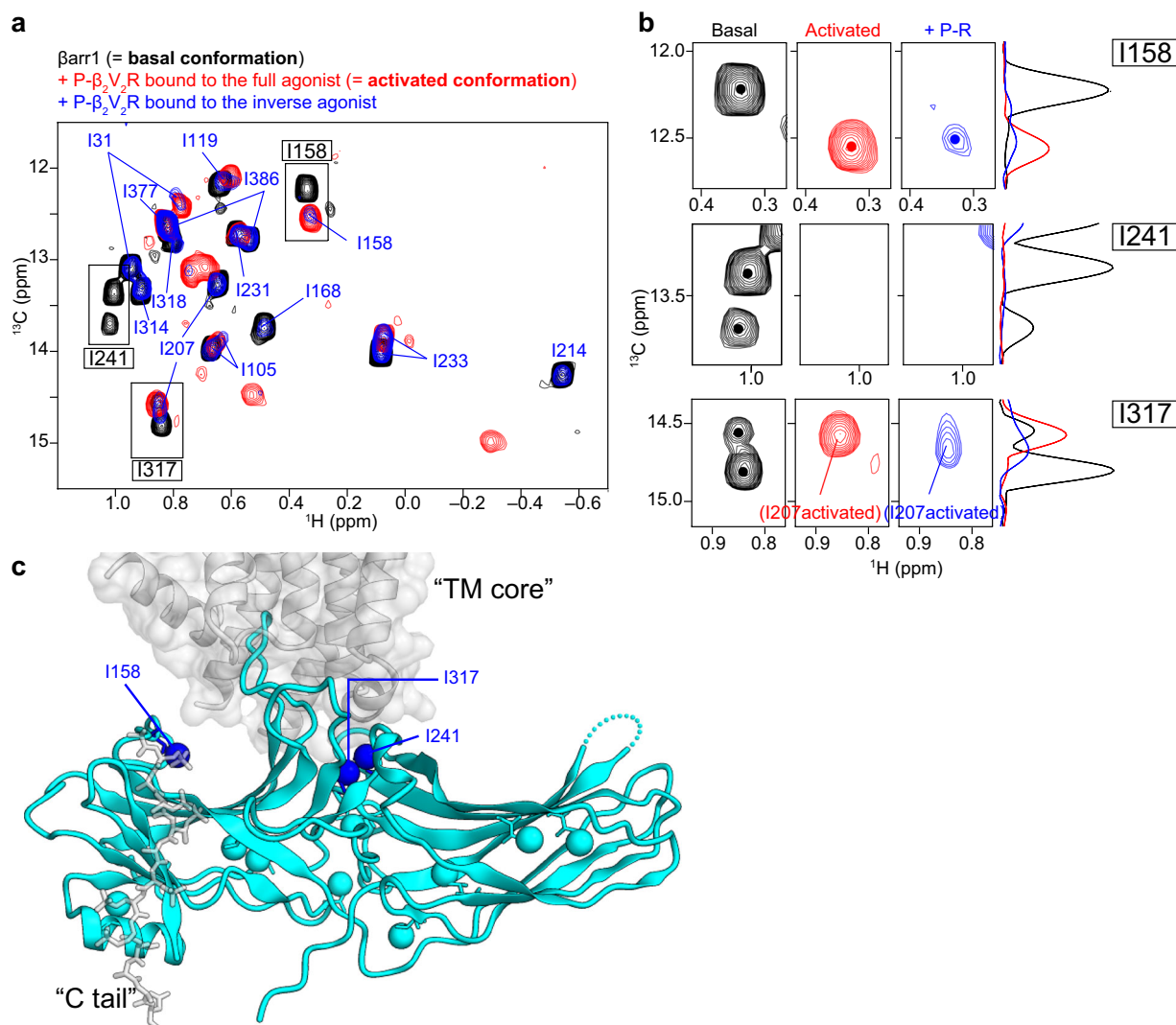


**Fig. 3** Conformational change of βarr1 upon binding to phosphorylated β<sub>2</sub>V<sub>2</sub>R bound to the inverse agonist. **a** Overlay of the <sup>1</sup>H-<sup>13</sup>C HMQC spectra of [u-<sup>2</sup>H, Ileδ1-<sup>13</sup>C<sup>1</sup>H<sub>3</sub>] βarr1 in the basal state (black), the complex with phosphorylated β<sub>2</sub>V<sub>2</sub>R in rHDLs bound to the full agonist (red), and the complex with phosphorylated β<sub>2</sub>V<sub>2</sub>R in rHDLs bound to the inverse agonist (blue). **b** Magnified views of resonances from I158 (upper row), I241 (middle row), and I317 (lower row) in the basal conformation (black), the activated conformation (red), and in the complex with phosphorylated β<sub>2</sub>V<sub>2</sub>R bound to the inverse agonist (blue). The <sup>13</sup>C 1D projections of selected regions are shown on the right of the spectra. The resonance from I158 exhibited a chemical shift change, and the resonances from I241 and I317 disappeared upon the addition of phosphorylated β<sub>2</sub>V<sub>2</sub>R in rHDLs bound to the inverse agonist. The split of the resonances from I241 and I317 in the basal state indicated the local conformational exchange, which is distinct from the exchange between the basal and activated conformations. **c** Mapping of the methyl groups adopting the activated conformation, in the complex of phosphorylated β<sub>2</sub>V<sub>2</sub>R bound to the inverse agonist, on the structure of βarr1 in complex with β<sub>1</sub>AR-V2R<sub>6P</sub> and Fab30 (PDB ID: 6TKO). Methyl groups exhibiting chemical shift changes or signal disappearance upon binding to phosphorylated β<sub>2</sub>V<sub>2</sub>R in rHDLs bound to the inverse agonist are indicated.

activated conformation, even though the C tail phosphorylation states are retained (Figs. 3 and 5). These results suggest that while the C tail interaction determines the affinity of the complex formation, the TM core interaction plays a crucial role to regulate the conformational changes for βarr1 activation. This agrees with the fact that some GPCRs, which are poorly phosphorylated by GRKs, transiently bind to βarrs but sufficiently activate the signal transduction by the TM core interaction<sup>13,30</sup>. Based on these results, we propose the following biphasic activation model: βarrs first bind to the phosphorylated C tail, which induces local conformational changes around the TM core-binding region, thus enabling the subsequent TM core interaction that stabilizes the activated conformation.

Even though the TM core interaction is attenuated by the inverse agonist, the binding of the conformation-selective antibody fragment, Fab30, can promote βarr1 to adopt the activated-

like conformation, which is similar to the activated conformation (Figs. 4b and 5). This is in good agreement with the fact that βarr1 adopts an activated conformation in the crystal structure of the βarr1-V2Rpp-Fab30 complex, in which the TM core interactions do not exist<sup>20</sup>. Since the addition of Fab30 in the absence of phosphorylated β<sub>2</sub>V<sub>2</sub>R did not induce significant chemical shift perturbations of the βarr1 resonances, prior interaction with the receptor would be required for Fab30-induced stabilization of the activated-like conformation (Supplementary Fig. 8). The Fab30-induced conformational change toward the activated-like conformation in the absence of the TM core interaction provides a good rationale for the allosteric potentiation of the interaction between βarr1-V2Rpp and ERK2 upon Fab30 binding<sup>31</sup>. Since the extent of the TM core-mediated interaction with βarrs varies among different GPCRs<sup>32</sup>, Fab30 may modulate the βarr-mediated signal transduction through GPCRs that poorly

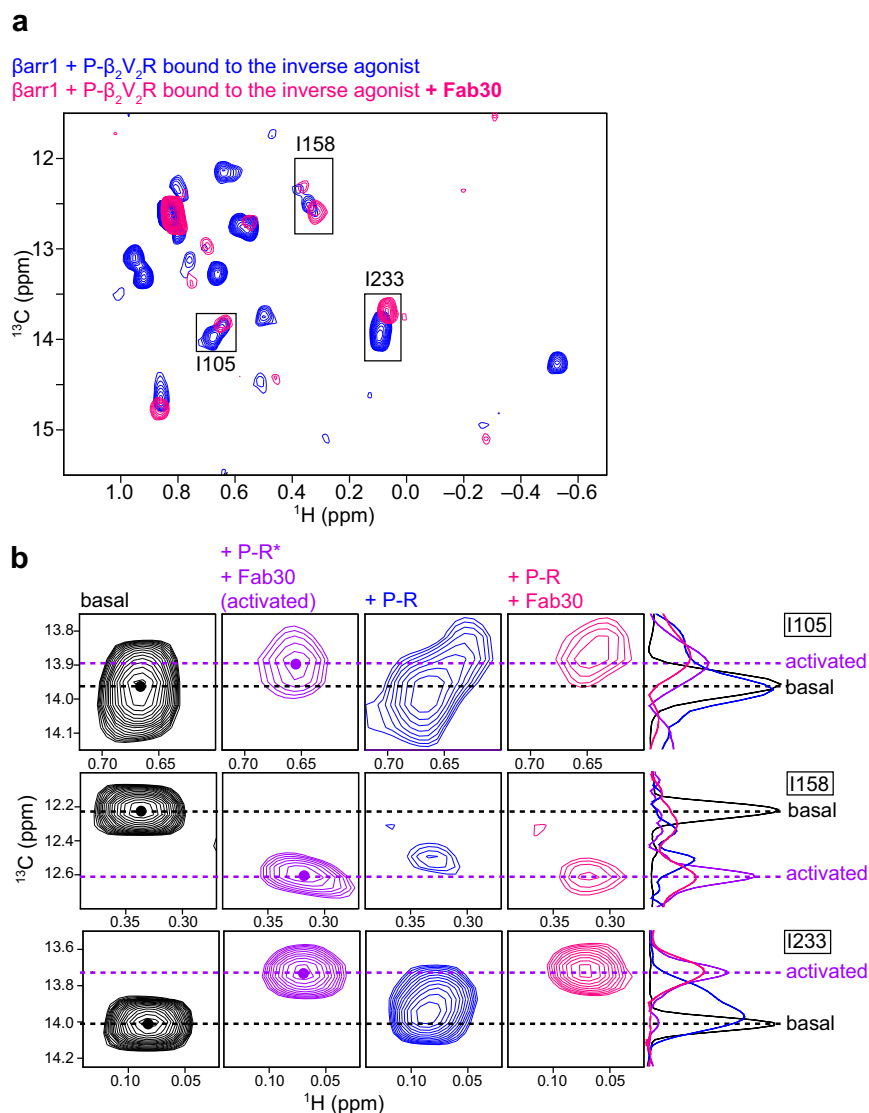


**Fig. 4** Effects of Fab30 on the  $\beta$ arr1 conformation in complex with phosphorylated  $\beta_2V_2R$  bound to the inverse agonist. **a** Overlay of the  $^1H$ - $^{13}C$  HMQC spectra of [ $u$ - $^2H$ , Ile $\delta$ 1- $^{13}C$ ] $H_3$   $\beta$ arr1 in the complex with phosphorylated  $\beta_2V_2R$  in rHDLs bound to the inverse agonist (blue) and in the complex with both phosphorylated  $\beta_2V_2R$  in rHDLs bound to the inverse agonist and Fab30 (pink). **b** Comparison of the resonances from the Ile $\delta$ 1 methyl groups of  $\beta$ arr1 in the basal state (black), in the complex with both phosphorylated  $\beta_2V_2R$  in rHDLs bound to the full agonist and Fab30 (+P-R\* + Fab30, purple), in the complex with phosphorylated  $\beta_2V_2R$  in rHDLs bound to the inverse agonist (+P-R, blue), and in the complex with both phosphorylated  $\beta_2V_2R$  in rHDLs bound to the inverse agonist and Fab30 (+P-R + Fab30, pink). The  $^{13}C$  1D projections of selected regions are shown on the right of the spectra. The 1D projection of the spectra corresponding to the basal state is reduced by a factor of five, to compare the  $^{13}C$  chemical shifts clearly. The  $^{13}C$  chemical shifts corresponding to the basal and activated conformations are indicated by dashed lines.

interact with  $\beta$ arr through the TM core, suggesting potential therapeutic applications.

Our results are closely related to the two different binding modes of the GPCR- $\beta$ arr complex: fully-engaged state, in which the receptor interacts with  $\beta$ arr through both the C tail and TM core, and partially-engaged state, in which the receptor only interacts with  $\beta$ arr through the C tail<sup>2,19</sup>. The present methyl-TROSY analyses demonstrated that the  $\beta$ arr1 binding mode, in complex with phosphorylated  $\beta_2V_2R$  in rHDLs bound to the inverse agonist, corresponds to the partially-engaged state, since  $\beta$ arr1 in the complex did not affect the conformation of the TM region of phosphorylated  $\beta_2V_2R$  in the inverse agonist-bound state (Supplementary Fig. 4). According to the methyl-TROSY analyses,  $\beta$ arr1 in the partially-engaged state exhibited limited activation, and exists in equilibrium between the major basal and minor activated conformations (Figs. 3a and 5). Considering the

fact that the partially-engaged state is reportedly competent with respect to several  $\beta$ arr-mediated responses, such as receptor internalization and c-Src activation<sup>2,4,5</sup>, a small population of the activated conformation is sufficient to recruit the signaling partners related to these responses. The stabilization of the activated conformation in the fully-engaged state observed in the present study may be required to recruit other signaling proteins with lower affinities for  $\beta$ arr.

The ability of synthetic GPCR ligands to induce signal transduction preferentially through either G protein or arrestin, a phenomenon known as biased agonism or functional selectivity, affects the therapeutic properties of ligands and is thus important for drug development<sup>33</sup>. Therefore, characterizations of both the G protein- and arrestin-mediated signaling activities are required to develop drugs targeting GPCRs. In most cases,  $\beta$ arr-mediated signaling activities are evaluated by cell-based  $\beta$ arr-recruitment

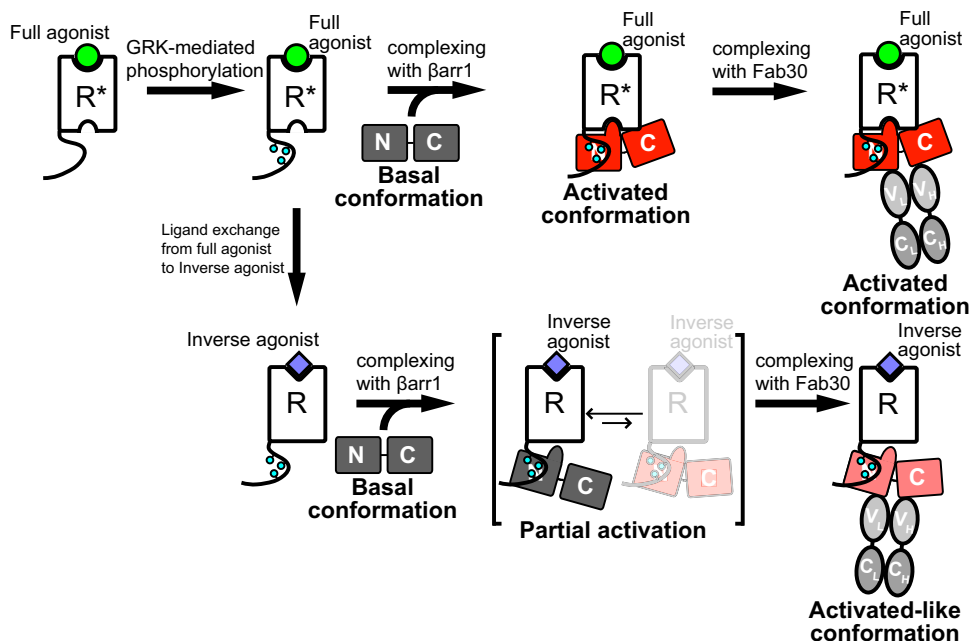


**Fig. 5 Conformational activation of  $\beta$ arr1 upon binding to GPCRs and the synthetic antibody fragment Fab30.** The full agonist-bound receptor is phosphorylated by GRK. The phosphorylated and full agonist-bound receptor interacts with  $\beta$ arr1 through both the TM core and C tail, and  $\beta$ arr1 in the complex adopts the activated conformation. Fab30 binding to the complex does not induce significant conformational changes in  $\beta$ arr1. In the case where the full agonist is replaced with the inverse agonist after GRK-mediated phosphorylation, the receptor only interacts with  $\beta$ arr1 through the C tail, resulting in partial activation in which  $\beta$ arr1 exists in equilibrium between the basal and activated conformations. Fab30 binding to the complex promotes  $\beta$ arr1 to adopt the activated-like conformation, which is partly similar to the activated conformation.

assays, which primarily reflect the ligand-induced GRK-mediated phosphorylation rather than the TM core interaction. Our NMR analyses suggest that the TM core interaction is critical to evaluate the conformational activation of  $\beta$ arr, which would be involved in engaging scaffolding partners. Considering the fact that GPCR ligands control the conformational equilibrium of the transmembrane region<sup>34,35</sup>, thus affecting the TM core interaction with  $\beta$ arr, this interaction and subsequent conformational change of  $\beta$ arr should also be evaluated to fully characterize the  $\beta$ arr-mediated signal transduction properties of ligand of interest.

Zhuang *et al.* previously reported a solution NMR investigation of the interactions between visual arrestin ( $\text{varr}$ ), a different subtype from  $\beta$ arr1, and its cognate GPCR rhodopsin in various phosphorylated and activated states<sup>15</sup>. The dark phosphorylated rhodopsin, which was assumed to interact with  $\text{varr}$  only through the C tail, induced chemical shift changes of the amide resonances from the C-terminal region of  $\text{varr}$  and the disappearance of the amide resonances from residues around the TM core-binding region. Moreover, Mayer *et al.* reported that phosphopeptides corresponding to the C tail of rhodopsin induced chemical shift changes of the amide resonances from the C-terminal and finger loop regions of  $\text{varr}$ , and some were split into two resonances, with one corresponding to the basal state<sup>36</sup>. These observations are in line with our results obtained with  $\beta$ arr1 in the complex with phosphorylated  $\beta_2\text{V}_2\text{R}$  bound to the inverse agonist (Fig. 3), suggesting that the effects of C tail interactions on the conformation could be conserved between  $\text{varr}$  and  $\beta$ arr1. However, light-activated phosphorylated rhodopsin, which was assumed to interact with  $\text{varr}$  through both the TM core and C tail, induced the disappearance of most of the amide and methyl resonances from  $\text{varr}$ , except for those from the C-terminal region, suggesting that  $\text{varr}$  bound to light-activated phosphorylated rhodopsin adopted a dynamic molten globule-like structure<sup>15</sup>. This contrasts with our observation that the methyl resonances from

$\beta$ arr1, in the complex with phosphorylated  $\beta_2\text{V}_2\text{R}$  bound to the full agonist, could be detected at chemical shifts corresponding to those stabilized by Fab30 (Fig. 2b and c), suggesting that the conformation of  $\beta$ arr1 induced by both the TM core and C tail would be more rigid than that of  $\text{varr}$ .

Previous conformational analyses of  $\beta$ arrs by solution NMR were based on the site-specific incorporations of unnatural amino acids, such as 3,5-difluorotyrosine (F2Y) and 4-trimethylsilylphenylalanine (TMSiPhe), through genetic code expansion<sup>37,38</sup>. The resonances from these unnatural amino acid sidechains minimally overlap with those derived from proteins and thus can be analyzed in 1D NMR experiments, enabling the rapid detection of conformational change around the labeled site. Using the TMSiPhe probe incorporated into position H295, near the polar core of  $\beta$ arr1, Liu *et al.* investigated the effect of the TM core of phosphorylated  $\beta_2\text{V}_2\text{R}$  on the conformation around the polar core. They reported that the volume of the resonances corresponding to the active state correlated well with the potency of the ligand, suggesting that the TM core interactions could induce conformational changes around the polar core<sup>38</sup>. Although our Ile probe was located at a different position, the resonance from Ile168, which is also close to the polar core, exhibited a similar ligand-dependent shift from the basal to activated state (Fig. 3). Thus, the present and previous observations are consistent. Our methyl-TROSY analyses also revealed that the TM core-mediated conformational change of  $\beta$ arr1 occurs not only around the polar core, but throughout the entire  $\beta$ arr1 structure.

Pharmacological analyses demonstrated that the allosteric effects of the agonist affinity, induced by  $\beta$ arr1 coupling, vary among different GPCRs<sup>32</sup>. Furthermore, several structures of GPCR- $\beta$ arr1 complexes revealed the different orientations of  $\beta$ arr1 with respect to the transmembrane region of GPCRs, although the common  $\beta$ arr1 regions are involved<sup>9–12</sup>. Thus, the degree of TM core-induced conformational activation observed in the present study may also vary among different GPCRs. In



addition, conformational analyses based on the Fab30 reactivity suggested that different conformational changes may occur in  $\beta$ arr1 versus  $\beta$ arr2 upon the TM core interaction<sup>39</sup>. Further structural analyses will clarify the details of TM core-induced conformational activation in the GPCR- $\beta$ arr signaling axis.

## Methods

**Reagents and buffers.** All reagents were from Nacalai Tesque, Inc., or Wako Chemicals unless otherwise noted.

**Generation of recombinant baculovirus expressing  $\beta_2V_2R$ .** The complementary DNA fragment encoding human  $\beta_2AR$  (Met1-C341), with the previously reported mutation (E122W/N187E/C265A)<sup>34</sup>, an N-terminal FLAG-tag (DYKDDDDA) and a C-terminal V2R C tail (A343-S371) was cloned into the pFastBac1 vector (Invitrogen). The hemagglutinin signal sequence (MKTIIALSIFCLVFA) was inserted immediately 5' to the FLAG tag. Sf9 cells (Invitrogen) were routinely maintained at 27 °C in Grace's supplemented insect cell medium (GIBCO) containing 10% fetal bovine serum (Biowest), 0.1% Pluronic F-68 (GIBCO), 50 International Units mL<sup>-1</sup> penicillin, 50  $\mu$ g mL<sup>-1</sup> streptomycin, and 0.125  $\mu$ g mL<sup>-1</sup> amphotericin B. The recombinant baculovirus was generated and amplified with the Bac-to-Bac system (Invitrogen), according to the manufacturer's instructions.

**Expression and purification of  $\beta_2V_2R$ .** The *expresSF* + cells (SF + cells, Protein Science Corp.) were routinely maintained in 100 mL Sf-900 II serum-free medium (GIBCO) in a 250 mL Erlenmeyer flask (Corning), at 27 °C on an orbital shaker (130 rpm). For  $\beta_2V_2R$  expression, the culture was expanded to 3 L. When the cell density reached about  $2 \times 10^6$  cells mL<sup>-1</sup>, 120 mL high-titer virus stocks, 1  $\mu$ M alprenolol (Sigma-Aldrich), and 14  $\mu$ M E-64 (Peptide Institute, Inc.) were added, and the culture was continued. Cells were harvested 48 h post-infection by centrifugation at 800  $\times$  g, and the resulting cell pellets were flash-frozen with liquid nitrogen and stored at -80 °C until use.

All of the following procedures were performed either on ice or in the cold room (4 °C). The cell pellet from 3 L of cell culture was suspended in 300 mL of buffer containing 10 mM HEPES-NaOH (pH 7.2), 20 mM KCl, 10 mM MgCl<sub>2</sub>, 0.1 mM tris (2-carboxyethyl) phosphine (TCEP), 1 mM 4-(2-aminoethyl) benzenesulfonyl fluoride hydrochloride (AEBSF), 20  $\mu$ M leupeptin hemisulfate (Peptide Institute, Inc.), 28  $\mu$ M E-64 (Peptide Institute, Inc.), and 0.3  $\mu$ M aprotinin (Wako Chemicals). The cells were disrupted by nitrogen cavitation (Parr Bomb) under 600 psi for 30 min, and the cell lysate was centrifuged at 142,000  $\times$  g for 45 min. The resulting pellet was washed twice with 80 mL buffer containing 10 mM HEPES-NaOH (pH 7.2), 1 M NaCl, 20 mM KCl, 10 mM MgCl<sub>2</sub>, 0.1 mM TCEP, 1 mM AEBSF, 20  $\mu$ M leupeptin hemisulfate, and 28  $\mu$ M E-64, and centrifuged at 142,000  $\times$  g for 45 min. The membrane pellet was resuspended in HBSG buffer (20 mM HEPES-NaOH (pH 7.2), 150 mM NaCl, 20% (w/v) glycerol, 0.1 mM TCEP), flash-frozen with liquid nitrogen, and stored at -80 °C.

The membrane pellet from 3 L of cell culture was solubilized for 3 h in 80 mL HBSG buffer supplemented with 1% *n*-dodecyl- $\beta$ -D-maltopyranoside (DDM, Dojindo), and was then centrifuged at 142,000  $\times$  g for 60 min. The supernatant was supplemented with 10 mM CaCl<sub>2</sub> and batch incubated with 8 mL ANTI-FLAG M1 Affinity Agarose Gel (Sigma-Aldrich). The resin was washed with 100 mL HBSG buffer supplemented with 0.1% DDM and 3 mM CaCl<sub>2</sub>. The protein was eluted with 20 mL HBSG buffer supplemented with 0.1% DDM, 5 mM EDTA, and 0.1 mg mL<sup>-1</sup> DYKDDDDK peptide (Wako Chemicals). The eluted  $\beta_2V_2R$  was concentrated to ~0.5 mL with Amicon Ultra-15 filters (50 kDa molecular weight cut-off, Millipore) and further purified by size exclusion chromatography on a Superose 6 10/300 GL column (GE Healthcare), equilibrated in buffer containing 20 mM HEPES-NaOH (pH 7.2), 150 mM NaCl, 0.1 mM TCEP, and 20  $\mu$ M formoterol (Toronto Research Chemicals). The eluted  $\beta_2V_2R$  was concentrated to ~0.5 mL with Amicon Ultra-4 filters (30 kDa molecular weight cut-off, Millipore), flash-frozen with liquid nitrogen, and stored at -80 °C until use.

**Preparation of GRK2.** The complementary DNA fragment encoding human GRK2 with a C-terminal hexahistidine-tag was cloned into the pFastBac1 vector (Invitrogen). The recombinant baculovirus was generated and amplified with the Bac-to-Bac system (Invitrogen), according to the manufacturer's instructions. The SF + cells were collected and resuspended in Sf-900 II serum-free medium (GIBCO) at a final cell density of  $2 \times 10^6$  cells mL<sup>-1</sup>. A 12 mL portion of the high-titer virus stock was added to 300 mL of the SF + cell culture, and the culture was continued at 27 °C. The cells were harvested 48 h post-infection by centrifugation at 800  $\times$  g, and the resulting cell pellets were flash-frozen with liquid nitrogen and stored at -80 °C until use.

All of the following procedures were performed either on ice or in the cold room (4 °C). The cell pellet was resuspended in 100 mL of buffer, containing 20 mM HEPES-NaOH (pH 7.2), 300 mM NaCl, and 0.02% Triton-X100. The cells were disrupted by sonication, and the cell lysate was centrifuged at 100,000  $\times$  g for 1 h. The supernatant was mixed with 4 mL of TALON metal affinity resin (Clontech) and batch incubated at 4 °C for 2 h. The resin was washed with 100 mL of buffer, containing 20 mM HEPES-NaOH (pH 7.2), 300 mM NaCl, and 10 mM

imidazole. The protein was eluted with 20 mL HEPES-NAOH (pH 7.2), 300 mM NaCl, and 200 mM imidazole. The eluate was concentrated with Amicon Ultra-15 filters (50 kDa molecular weight cut-off, Millipore), and further purified by size exclusion chromatography on a Superdex 200 10/300 GL Increase column (GE Healthcare), equilibrated in buffer containing 20 mM HEPES-NaOH (pH 7.2), 300 mM NaCl, 2 mM EDTA, and 1 mM DTT. The eluted GRK2 was flash-frozen with liquid nitrogen, and stored at -80 °C until use.

**Reconstitution of  $\beta_2V_2R$  into rHDLs.** The *Escherichia coli* BL21 (DE3) (Stratagene), transformed with the plasmid encoding His-tagged MSP1D1 or MSP1E3D1, was cultured at 37 °C in Terrific Bloth (TB) media containing 100 mg L<sup>-1</sup> of ampicillin. When the culture attained an OD<sub>600</sub> of 2.0, 1 mM of IPTG was added to induce protein expression and the culture was continued further at 37 °C for 3 h. The cells were harvested by centrifugation at 5000  $\times$  g for 15 min, and the resulting cell pellets were stored at -80 °C. The cells were suspended in buffer containing 50 mM Tris-HCl (pH7.5), 300 mM NaCl, 100 mM KCl, and disrupted by sonication. The cell lysate was centrifuged at 20,000  $\times$  g for 30 min, and the pellet was suspended in buffer containing 50 mM Tris-HCl (pH7.5), 300 mM NaCl, 100 mM KCl, 1% Triton X-100. The suspension was centrifuged at 100,000  $\times$  g for 1 h, and the supernatant was applied to HIS-Select resin (SIGMA). The resin was washed with buffer containing 50 mM Tris-HCl (pH7.5), 300 mM NaCl, 100 mM KCl, 50 mM Na-cholate, 20 mM imidazole. The His-tagged MSP1D1 or MSP1E3D1 was eluted with buffer containing 50 mM Tris-HCl (pH7.5), 300 mM NaCl, 100 mM KCl, 200 mM imidazole. Afterward, TEV protease was added to the eluate, which was dialyzed against buffer, containing 50 mM Tris-HCl, 10 mM NaCl, 0.5 mM EDTA for 1 day. The sample was then dialyzed against buffer, containing 20 mM HEPES-NaOH (pH 7.2), 150 mM NaCl, and passed through the HIS-Select resin to obtain the MSP1D1 or MSP1E3D1 without His-tag. Since better NMR spectra were obtained when using MSP1D1, we used it to construct rHDLs, except for the NMR experiment in Supplementary Fig. 9 (see Supplementary Note 1 for details).

A mixture of 1-palmitoyl-2-oleoyl-phosphatidylcholine (POPC, Avanti Polar Lipids) and 1-palmitoyl-2-oleoyl-phosphatidylglycerol (POPG, Avanti Polar Lipids) in chloroform was prepared at a molar ratio of 3:2. The solvent was evaporated under a nitrogen atmosphere and dried *in vacuo* to form a lipid film. The film was solubilized in buffer, containing 20 mM HEPES-NaOH (pH 7.2), 150 mM NaCl, 0.1 mM TCEP, and 100 mM sodium cholate, for a final lipid concentration of 50 mM.

All of the following procedures were performed either on ice or in the cold room (4 °C) unless otherwise stated. The MSP1D1 and the lipid solution were added to the prepared  $\beta_2V_2R$  in DDM micelles at final concentrations of 0.1 mM and 5 mM, respectively. The mixture was incubated on ice for at least 3 h. Afterwards, 80% (w/v) of Bio-Beads SM-2 (Bio-Rad) was added to the mixture and incubated at 4 °C overnight with gentle mixing. The supernatant was supplemented with 10 mM CaCl<sub>2</sub>, and applied to a 2 mL ANTI-FLAG M1 Affinity Agarose Gel column, equilibrated in HBSG buffer supplemented with 3 mM CaCl<sub>2</sub>. The resin was washed with 40 mL HBSG buffer supplemented with 3 mM CaCl<sub>2</sub>. The  $\beta_2V_2R$  in rHDLs was eluted with HBSG buffer supplemented with 5 mM EDTA, 0.2 mg mL<sup>-1</sup> DYKDDDDK peptide, and 20  $\mu$ M formoterol, and concentrated to ~0.5 mL with Amicon Ultra-4 filters (10 kDa molecular weight cut-off, Millipore).

For the preparation of phosphorylated  $\beta_2V_2R$ , the buffer was exchanged to 20 mM Tris-HCl, pH 7.5, 10 mM MgCl<sub>2</sub>, and 0.1 mM TCEP, using a NAP-5 desalting column (GE Healthcare). Purified GRK2, ATP, and formoterol were added at final concentrations of 2  $\mu$ M, 1 mM, and 100  $\mu$ M, respectively. The reaction mixture was incubated at 30 °C for 2 h, and then analyzed by SDS-PAGE with Pro-Q Diamond (Molecular Probes) staining. Gel images were obtained with a Typhoon FLA 9000 imager (GE Healthcare).

The eluate from the ANTI-FLAG M1 Affinity Agarose Gel or the phosphorylation reaction mixture was further purified by size exclusion chromatography on a Superdex 200 10/300 GL Increase column (GE Healthcare), equilibrated in 20 mM HEPES-NaOH (pH 7.2), 150 mM NaCl, 0.1 mM TCEP, and 10  $\mu$ M formoterol. The eluate was concentrated with Amicon Ultra-4 filters (10 kDa molecular weight cut-off, Millipore), and the buffer was exchanged to 20 mM HEPES-NaOH (pH 7.0), 150 mM NaCl, 0.1 mM TCEP, and 50  $\mu$ M formoterol, in 100% D<sub>2</sub>O.

To prepare phosphorylated  $\beta_2V_2R$  bound to carazolol, the unbound formoterol was removed by using a NAP-5 desalting column (GE Healthcare), and then 100  $\mu$ M carazolol was added. The reaction was incubated at 298 K for at least 16 h.

**Preparation of isotope-labeled  $\beta$ -arrestin.** The complementary DNA fragment encoding the hexahistidine-tag, the TEV protease-cleavage site (ENLYFQG), and the human  $\beta$ -arrestin 1 cysteine-less mutant<sup>16</sup> was cloned into the pTrcHisB vector (Thermo Fisher Scientific). The resulting protein sequence was: MGGSHHHHHHGMASENLYFQ/GMGDKGTRVFKKASPNGKLTVYLGRDFV DHIDLVDVDPVGVVLDPEYLKERRVYVLTVAFRYGRDLVDVGLTFRKDLF VANVQSFPPAPEDKPKLTRLQERLIKRLGHEHAYPFTFEIPPNLPSVTLQGPED TKGALGVDDYEVKAFVAENLEEKIKHNSVRLVIRKVFQYAPERPGPQPTAETT RQFLMSDKPLHLEASLDKEIYYHGEPISVNVHVTNNTNKTVKKIKISVRQYAD IVLNFNTAQYKVPVAMEEADDTVAPSSTFSKYVTLTPFLANNREKRGLALDGGK LKHEDTNLASSTLLREGANREILGIHVSYKVKVLLVSRGGLLDLASSDVAVE

LPFTLMHPKPKKEPPHREVPENETPVDTNLIELDTNDDDDIVFEDFARQLKGMKDDKEEEEDGTGSPQLNRR, where the TEV protease cleaves between Q and G in the cleavage site. Further mutations were introduced by PCR-based site-directed mutagenesis to generate  $\beta$ arr1 variants for the resonance assignments of the isoleucine  $\delta$ 1 methyl group. The sequences of the oligonucleotides used to generate the  $\beta$ arr1 variants are listed in Supplementary Table 1. The *Escherichia coli* (*E. coli*) BL21 (DE3) Codon Plus RP strain (Stratagene), transformed with the prepared plasmid was cultured overnight at 37 °C in 10 mL Luria Bertani (LB) medium containing 100 mg L<sup>-1</sup> ampicillin. The overnight culture was used to inoculate 1 L of D<sub>2</sub>O-based M9 medium, supplemented with 2 g L<sup>-1</sup> [<sup>2</sup>H<sub>7</sub>] glucose (Cambridge Isotope Laboratories) and 1 g L<sup>-1</sup> [<sup>15</sup>NH<sub>4</sub>Cl] (SI Science Co., Ltd.). When the culture attained an OD<sub>600</sub> of 0.8, 0.3 mM isopropyl- $\beta$ -D-thiogalactopyranoside (IPTG) was added to induce protein expression and the culture was further incubated at 30 °C for 20 h. For selective [<sup>13</sup>C]<sub>3</sub> labeling of the isoleucine  $\delta$ 1 methyl group, the medium was supplemented with 50 mg L<sup>-1</sup> of [methyl-<sup>13</sup>C, 3,3-<sup>2</sup>H] ketobutyric acid (Cambridge Isotope Laboratories), 1 h before the IPTG addition<sup>28</sup>. The cells were harvested by centrifugation at 5000 × g for 15 min, and the resulting cell pellets were flash-frozen with liquid nitrogen and stored at -80 °C until use.

The cells from a 1 L culture were suspended in 60 mL of 20 mM Tris-HCl (pH 8.0) and 200 mM NaCl, supplemented with Protease Inhibitor Cocktail. The cells were disrupted by sonication, and the cell lysate was centrifuged at 100,000 × g for 1 h. The supernatant was applied to a 1 mL HisTrap HP column (GE Healthcare), equilibrated in buffer containing 20 mM Tris-HCl (pH 8.0) and 200 mM NaCl. The protein was eluted by a linear concentration gradient of imidazole, from 25 mM to 175 mM. Afterwards, 1 mg of TEV protease was added to the eluate, which was dialyzed for 16–18 h against buffer containing 20 mM Tris-HCl (pH 8.0), 150 mM NaCl, and 2 mM EDTA. The samples were applied to a 1 mL HiTrap Heparin HP column (GE Healthcare), equilibrated with buffer containing 20 mM Tris-HCl (pH 8.0), 150 mM NaCl, and 2 mM EDTA. The protein was eluted by a linear concentration gradient of NaCl, from 200 mM to 700 mM. The eluate was concentrated with Amicon Ultra-4 filters (30 kDa molecular weight cut-off, Millipore), and further purified by size exclusion chromatography on a Superdex 75 10/300 GL column (GE Healthcare), equilibrated in buffer containing 20 mM Tris-HCl (pH 8.0), 300 mM NaCl, and 2 mM EDTA. The eluate was concentrated with Amicon Ultra-4 filters (10 kDa molecular weight cut-off, Millipore), and the buffer was exchanged to 20 mM HEPES-NaOH (pH 7.0), 150 mM NaCl, 0.1 mM TCEP, and 50  $\mu$ M  $\beta$ <sub>2</sub>AR ligand (formoterol or carazolol), 100% D<sub>2</sub>O.

**Surface plasmon resonance experiments.** The  $\beta$ arr1 binding activities of unphosphorylated and phosphorylated  $\beta$ <sub>2</sub>V<sub>2</sub>R were analyzed with a Biacore T200 instrument (GE Healthcare). The  $\beta$ <sub>2</sub>V<sub>2</sub>Rs embedded in biotinylated rHDLs were captured on flow cells with the Series S Sensor Chip SA (GE Healthcare), via the interaction between biotin and streptavidin. The binding assays were carried out in buffer containing 20 mM HEPES-NaOH (pH 7.2), 150 mM NaCl, and 1  $\mu$ M formoterol or carazolol, at a flow rate of 30  $\mu$ L min<sup>-1</sup>. The sensorgrams were processed with the Biacore T-200 Evaluation software (GE Healthcare).

**Preparation of Fab30.** *E. coli* 55244 cells (ATCC) were transformed with the Fab30 plasmid, and single colonies were inoculated in 50 mL of 2×YT media and grown overnight at 30 °C as the primary culture. On the next day, secondary cultures were inoculated in fresh 2×YT media with 5% volume of primary culture and grown for 8 h at 30 °C. The cells were then centrifuged, resuspended in an equal volume of CRAP medium, and grown for 16 h at 30 °C. Cell pellets were harvested and stored at -80 °C until further use. For purification, cells were resuspended in lysis buffer (50 mM HEPES-Na<sup>+</sup> (pH 8.0), 0.5 M NaCl, 0.5% (v/v) Triton X-100, 0.5 mM MgCl<sub>2</sub>) and lysed by sonication. The cell lysate was heated at 65 °C in a water bath for 30 min, chilled on ice for 5 min, and then centrifuged at 20,000 × g for 30 min. The clarified cell lysate was loaded onto a pre-equilibrated Protein L column at room temperature, which was eluted by gravity flow at a rate of 1–2 mL min<sup>-1</sup>. The Protein L resin was extensively washed with wash buffer (50 mM HEPES-Na<sup>+</sup> (pH 8.0), 0.5 M NaCl), and the Fab30 protein was eluted with 100 mM acetic acid. Eluted fractions were neutralized immediately with 10% volume of neutralization buffer (1 M HEPES (pH 8.0)), and subsequently desalted and buffer-exchanged into storage buffer (20 mM HEPES-Na<sup>+</sup> (pH 8.0), 0.1 M NaCl) using PD-10 columns (GE Healthcare). Purified Fab30 was supplemented with 10% (v/v) glycerol, flash-frozen, and stored at -80 °C until further use. To assess the functionality of the purified Fab30, a co-immunoprecipitation assay was performed, in which the reactivity of Fab30 towards V2Rpp-bound  $\beta$ arr1 was used as readout. For this assay, purified Fab30 (2.5  $\mu$ g) was incubated with purified  $\beta$ arr1 (2.5  $\mu$ g) with or without V2Rpp (pre-incubation with  $\beta$ arr1 for 30 min on ice) in a 100–200  $\mu$ L reaction volume for 1 h at room temperature, and then pre-equilibrated Protein L beads were added. After an additional 1 h incubation at room temperature, the Protein L beads were washed 3–5 times with wash buffer (20 mM HEPES-Na<sup>+</sup> (pH 7.4), 150 mM NaCl, 0.01% (w/v) LMNG), and bound proteins were eluted using 2×SDS loading buffer. Eluted proteins were separated by SDS-PAGE and selective interactions of Fab30 with activated  $\beta$ arr1 were visualized by western blotting and Coomassie Brilliant Blue staining.

**NMR experiments.** All spectra were recorded with a Bruker AVANCE III 800 spectrometer equipped with a cryogenic probe, processed by Topspin 3.6.2 (Bruker), and analyzed by Sparky<sup>40</sup>. The <sup>1</sup>H chemical shifts were referenced to the methyl protons of 3-(trimethylsilyl)-1-propanesulfonic acid sodium salt, and the <sup>13</sup>C chemical shifts were referenced indirectly.

<sup>1</sup>H-<sup>13</sup>C heteronuclear multiple-quantum coherence (HMQC) spectra with echo/anti-echo gradient coherence selection were recorded for 15  $\mu$ M  $\beta$ arr1, in buffer containing 20 mM HEPES-NaOH (pH 7.2), 150 mM NaCl, and 50  $\mu$ M  $\beta$ <sub>2</sub>AR ligands prepared in D<sub>2</sub>O. The phosphorylated  $\beta$ <sub>2</sub>V<sub>2</sub>R and Fab30 were mixed at final concentrations of 30  $\mu$ M and 40  $\mu$ M, respectively. The spectral widths were set to 16 and 16 ppm for the <sup>1</sup>H and <sup>13</sup>C dimensions, respectively, and inter-scan delays were set to 1 sec. In total, 1,024 (<sup>1</sup>H) × 96 (<sup>13</sup>C) complex points were recorded, and 256 scans/FID gave rise to an acquisition time of 14 h for each spectrum. Prior to Fourier transformation, the data matrices were zero-filled to 2,048 (<sup>1</sup>H) × 128 (<sup>13</sup>C) complex points, and multiplied by a Gaussian apodization function in the <sup>1</sup>H dimension and a 60°-shifted squared sine bell apodization function in the <sup>13</sup>C dimension.

Normalized chemical shift differences of the Ile $\delta$ 1 methyl group,  $\Delta\delta$ , were calculated by the following equation:  $\Delta\delta = [(\Delta\delta_{1H})^2 + (\Delta\delta_{13C}/5.7)^2]^{0.5}$ . The normalization factor (5.7) is the ratio of the standard deviation of the isoleucine  $\delta$ 1 methyl <sup>1</sup>H and <sup>13</sup>C chemical shifts, deposited in the Biological Magnetic Resonance Data Bank (<http://www.bmrb.wisc.edu/>). The error values were calculated by the formula  $[\Delta\delta_{1H} R_{1H} + \Delta\delta_{13C} R_{13C}/(5.7)^2]/\Delta\delta$ , where  $R_{1H}$  and  $R_{13C}$  are the digital resolution in ppm in the <sup>1</sup>H and <sup>13</sup>C dimensions, respectively.

**Reporting summary.** Further information on research design is available in the Nature Research Reporting Summary linked to this article.

## Data availability

The data that support this study are available from the corresponding author upon reasonable request. The chemical shift data have been deposited in Biological Magnetic Resonance Bank under accession code 51131. The previously existing PDB entries 1G4M, 2RH1, and 6TKO were used in this study. Source data are provided with this paper.

Received: 6 August 2021; Accepted: 24 November 2021;

Published online: 09 December 2021

## References

- Hilger, D., Masureel, M. & Kobilka, B. K. Structure and dynamics of GPCR signaling complexes. *Nat. Struct. Mol. Biol.* **25**, 4–12 (2018).
- Cahill, T. et al. Distinct conformations of GPCR- $\beta$ -arrestin complexes mediate desensitization, signaling, and endocytosis. *Proc. Natl. Acad. Sci. USA* **114**, 2562–2567 (2017).
- De Vries, L. et al. Innovative bioluminescence resonance energy transfer assay reveals differential agonist-induced D2 receptor intracellular trafficking and arrestin-3 recruitment. *Mol. Pharmacol.* **96**, 308–319 (2019).
- Kumari, P. et al. Functional competence of a partially engaged GPCR- $\beta$ -arrestin complex. *Nat. Commun.* **7**, 13416 (2016).
- Kumari, P. et al. Core engagement with  $\beta$ -arrestin is dispensable for agonist-induced vasopressin receptor endocytosis and ERK activation. *Mol. Biol. Cell* **28**, 1003–1010 (2017).
- Han, M. et al. Crystal structure of  $\beta$ -arrestin at 1.9 Å: possible mechanism of receptor binding and membrane translocation. *Structure* **9**, 869–880 (2001).
- Ranjan, R. et al. Novel structural insights into GPCR- $\beta$ -arrestin interaction and signaling. *Trends Cell. Biol.* **27**, 851–862 (2017).
- Kang, Y. et al. Crystal structure of rhodopsin bound to arrestin by femtosecond X-ray laser. *Nature* **523**, 561–567 (2015).
- Staus, D. P. et al. Structure of the M2 muscarinic receptor- $\beta$ -arrestin complex in a lipid nanodisc. *Nature* **579**, 297–302 (2020).
- Huang, W. et al. Structure of the neurotensin receptor 1 in complex with  $\beta$ -arrestin 1. *Nature* **579**, 303–308 (2020).
- Lee, Y. et al. Molecular basis of  $\beta$ -arrestin coupling to formoterol-bound  $\beta$ <sub>1</sub>-adrenoceptor. *Nature* **583**, 862–866 (2020).
- Yin, W. et al. A complex structure of arrestin-2 bound to a G protein-coupled receptor. *Cell Res.* **29**, 971–983 (2019).
- Eichel, K. et al. Catalytic activation of  $\beta$ -arrestin by GPCRs. *Nature* **557**, 381–386 (2018).
- Latorraca, N. et al. Molecular mechanism of GPCR-mediated arrestin activation. *Nature* **557**, 452–456 (2018).
- Zhuang, T. et al. Involvement of distinct arrestin-1 elements in binding to different functional forms of rhodopsin. *Proc. Natl. Acad. Sci. USA* **110**, 942–947 (2013).
- Hanson, S. M. et al. Arrestin mobilizes signaling proteins to the cytoskeleton and redirects their activity. *J. Mol. Biol.* **368**, 375–387 (2007).

17. Oakley, R. H. et al. Association of  $\beta$ -arrestin with G protein-coupled receptors during clathrin-mediated endocytosis dictates the profile of receptor resensitization. *J. Biol. Chem.* **274**, 32248–32257 (1999).
18. Oakley, R. H. et al. Differential affinities of visual arrestin,  $\beta$ arrestin1, and  $\beta$  arrestin2 for G protein-coupled receptors delineate two major classes of receptors. *J. Biol. Chem.* **275**, 17201–17210 (2000).
19. Shukla, A. K. et al. Visualization of arrestin recruitment by a G-protein-coupled receptor. *Nature* **512**, 218–222 (2014).
20. Shukla, A. K. et al. Structure of active  $\beta$ -arrestin-1 bound to a G-protein-coupled receptor phosphopeptide. *Nature* **497**, 137–141 (2013).
21. Lally, C. et al. C-edge loops of arrestin function as a membrane anchor. *Nat. Commun.* **8**, 14258 (2017).
22. Bayburt, T., Grinkova, Y. & Sligar, S. Self-assembly of discoidal phospholipid bilayer nanoparticles with membrane scaffold proteins. *Nano Lett.* **2**, 853–856 (2002).
23. Komolov, K. et al. Structural and functional analysis of a  $\beta_2$ -adrenergic receptor complex with GRK5. *Cell* **169**, 407–421 (2017).
24. Sommer, M. E., Smith, W. C. & Farrens, D. L. Dynamics of arrestin-rhodopsin interactions: acidic phospholipids enable binding of arrestin to purified rhodopsin in detergent. *J. Biol. Chem.* **281**, 9407–9417 (2006).
25. Bayburt, T. H. et al. Monomeric rhodopsin is sufficient for normal rhodopsin kinase (GRK1) phosphorylation and arrestin-1 binding. *J. Biol. Chem.* **286**, 1420–1428 (2011).
26. Shiraishi, Y. et al. Phosphorylation-induced conformation of  $\beta_2$ -adrenoceptor related to arrestin recruitment revealed by NMR. *Nat. Commun.* **9**, 194 (2018).
27. Tugarinov, V. et al. Cross-correlated relaxation enhanced  $^1\text{H}$ - $^{13}\text{C}$  NMR spectroscopy of methyl groups in very high molecular weight proteins and protein complexes. *J. Am. Chem. Soc.* **125**, 10420–10428 (2003).
28. Goto, N. K. et al. A robust and cost-effective method for the production of Val, Leu, Ile ( $\delta$ 1) methyl-protonated  $^{15}\text{N}$ -,  $^{13}\text{C}$ -,  $^2\text{H}$ -labeled proteins. *J. Biomol. NMR* **13**, 369–374 (1999).
29. Nobles, K. et al. The active conformation of  $\beta$ -arrestin1—Direct evidence for the phosphate sensor in the N-domain and conformational differences in the active states of  $\beta$ -arrestins1 and -2. *J. Biol. Chem.* **282**, 21370–21381 (2007).
30. Eichel, K., Jullie, D. & von Zastrow, M.  $\beta$ -Arrestin drives MAP kinase signalling from clathrin-coated structures after GPCR dissociation. *Nat. Cell Biol.* **18**, 303–310 (2016).
31. Ghosh, E. et al. A synthetic intrabody-based selective and generic inhibitor of GPCR endocytosis. *Nat. Nanotechnol.* **12**, 1190–1198 (2017).
32. Staus, D. P. et al. Sortase ligation enables homogeneous GPCR phosphorylation to reveal diversity in  $\beta$ -arrestin coupling. *Proc. Natl. Acad. Sci. USA* **115**, 3834–3839 (2018).
33. Smith, J. S., Lefkowitz, R. J. & Rajagopal, S. Biased signalling: from simple switches to allosteric microprocessors. *Nat. Rev. Drug Discov.* **17**, 243–260 (2018).
34. Kofuku, Y. et al. Efficacy of the  $\beta_2$ -adrenergic receptor is determined by conformational equilibrium in the transmembrane region. *Nat. Commun.* **3**, 1045 (2012).
35. Imai, S. et al. Structural equilibrium underlying ligand-dependent activation of  $\beta_2$ -adrenoceptor. *Nat. Chem. Biol.* **16**, 430–439 (2020).
36. Mayer, D. et al. Distinct G protein-coupled receptor phosphorylation motifs modulate arrestin affinity and activation and global conformation. *Nat. Commun.* **10**, 1261 (2019).
37. Yang, F. et al. Phospho-selective mechanisms of arrestin conformations and functions revealed by unnatural amino acid incorporation and  $^{19}\text{F}$ -NMR. *Nat. Commun.* **6**, 8202 (2015).
38. Liu, Q. et al. Desipherring receptor core-induced and ligand-dependent conformational changes in arrestin via genetic encoded trimethylsilyl  $^1\text{H}$ -NMR probe. *Nat. Commun.* **11**, 4857 (2020).
39. Ghosh, E. et al. Conformational sensors and domain swapping reveal structural and functional differences between  $\beta$ -arrestin isoforms. *Cell. Rep.* **28**, 3287–3299 (2019).
40. Goddard, T. D. and D. G. Kneller, SPARKY 3, University of California, San Francisco.

### Acknowledgements

This work was supported by grants from Japan Society for the Promotion of Science (JSPS) KAKENHI grant number JP17H06097 (to I.S.), JP20H03375 (to T.U.), JP19H04951 (to T.U.), JP21H02410 (to Y.K.), JP20K21473 (to Y.K.), and JP19H04946 (to Y.K.); and the Japan Agency for Medical Research and Development (AMED) grant number JP18ae010104 (to I.S.). Research program in the laboratory of A.K.S. is supported by the Senior Fellowship of DBT/WT India Alliance (IA/S/20/1/504916). A.K.S. is EMBO Young Investigator and Joy Gill Chair Professor. H.D.-A. is supported by the BioCare scheme of the Department of Biotechnology (DBT: BT/PR31791/BIC/101/1228/2).

### Author contributions

Y.S., Y.K., T.U., A.K.S., and I.S. designed the research. Y.S. prepared  $\beta$ arr1 and various forms of  $\beta_2\text{V}_2\text{R}$  embedded in rHDLs, and performed SPR and NMR experiments. S.P. and H.D.-A. expressed, purified and characterized Fab30 under the supervision of A.K.S. Y.S., A.K.S., and I.S. analyzed the data and wrote the manuscript.

### Competing interests

The authors declare no competing interests.

### Additional information


**Supplementary information** The online version contains supplementary material available at <https://doi.org/10.1038/s41467-021-27482-3>.

**Correspondence** and requests for materials should be addressed to Ichio Shimada.

**Peer review information** *Nature Communications* thanks the anonymous reviewer(s) for their contribution to the peer review of this work. Peer reviewer reports are available.

**Reprints and permission information** is available at <http://www.nature.com/reprints>

**Publisher's note** Springer Nature remains neutral with regard to jurisdictional claims in published maps and institutional affiliations.

 **Open Access** This article is licensed under a Creative Commons Attribution 4.0 International License, which permits use, sharing, adaptation, distribution and reproduction in any medium or format, as long as you give appropriate credit to the original author(s) and the source, provide a link to the Creative Commons license, and indicate if changes were made. The images or other third party material in this article are included in the article's Creative Commons license, unless indicated otherwise in a credit line to the material. If material is not included in the article's Creative Commons license and your intended use is not permitted by statutory regulation or exceeds the permitted use, you will need to obtain permission directly from the copyright holder. To view a copy of this license, visit <http://creativecommons.org/licenses/by/4.0/>.

© The Author(s) 2021